The influence of RGO gain on Co 0.5 Mn 0.3 Cu 0.2 Fe 2 O 4 nano-composites' construction, morphology, and magnetic characteristics

Seyed Ali Hosseini Moradi
Malayer University
Nader Ghobadi (n.ghobadi@malayer.ac.ir)
Malayer University

Research Article

Keywords:

Posted Date: June 30th, 2022

DOI: https://doi.org/10.21203/rs.3.rs-1777017/v1

Abstract

One-pot simplified co-precipitation procedure was used to produce non-stoichiometric ferrite ($Co_{0.5}Mn_{0.3}Cu_{0.2}Fe_2O_4$) and diminish graphene oxide (rGO) nano-composites in this investigation. Powders such as XRD, FT-IR, and SEM were used to study the structural and surface analysis of the composites. An investigation of the magnetic characteristics of $Co_{0.5}Mn_{0.3}Cu_{0.2}Fe_2O_4$ nanocomposites (NCs) was also conducted using VSM. A vector network analysis tool was used to conduct microwave adsorption investigations on $Co_{0.5}Mn_{0.3}Cu_{0.2}Fe_2O_4$ NCs in the 2–18 GHz frequency spectrum. By adjusting the amount of rGO added to $Co_{0.5}Mn_{0.3}Cu_{0.2}Fe_2O_4$, the electromagnetic (EM) wave absorbing characteristics of $Co_{0.5}Mn_{0.3}Cu_{0.2}Fe_2O_4$ nanocomposites may be remarkably adaptable due to their customizable microstructure and synergistic effects. The addition of rGO can significantly improve EM wave absorption characteristics compared to the unadulterated $Co_{0.5}Mn_{0.3}Cu_{0.2}Fe_2O_4$ ferrites. The generated $Co_{0.5}Mn_{0.3}Cu_{0.2}Fe_2O_4$ NCs' minor reflection loss (RL) was 39.7 dB in the 11.9 GHz frequency spectrum. The effective absorption bandwidth is a maximum of 6.5 GHz (RL under 10 dB) with a thickness of two millimeters. The $Co_{0.5}Mn_{0.3}Cu_{0.2}Fe_2O_4$ NCs that haven't been changed since synthesis (: as-synthesized) might be considered a novel alternative for the slight EM wave absorber due to their proper impedance matching and synergistic effect **among** dielectric and magnetic loss.

1. Introduction

Over the last few years, electromagnetic (EM) wave interference has become a significant environmental pollution issue that can endanger people's health and the regular operation of electrical devices due to the widespread use of wireless communication gadgets, local area networks, and other communication supplies [1–3]. Such issues have effects not just on the regular operation of specific devices but also on people's health. To eliminate the damage caused by electromagnetic (EM) interference, significant work has been carried into manufacturing materials that can successfully absorb EM waves and convert EM energy into heat or microwave energy, which is employed to reduce interference damage [4–7]. Electrical science devices, military armaments, and other supplies are commonly utilized materials of this type, furthermore commercially accessible. Yet, developing and synthesizing EM wave absorbers with slight and narrow thickness, wide absorption bandwidth, and considerable absorption over a broad frequency spectrum remains a challenge [8–11]. Also, numerous prior studies have shown that traditional single-phase EM wave absorption materials, including ferrites, conductive polymers, ceramics, and metal powders, cannot match the aforementioned functional criteria [12, 13].

The production and investigation of spinel nano ferrite ($M^{2+}Fe_2O_4$, M^{2+} = Fe, Co, Mn, Cu) are more attractive among the many magnetic materials because their hard/soft magnetic nature is influenced by the form of divalent cation (M^{2+}) existing in nano ferrites [14–16]. $CoFe_2O_4$ stands out for its outstanding chemical stability, saturation magnetization (Ms), considerable coercivity, significant magneto crystalline anisotropy (MCA), tremendous magneto strictive coefficient, and mechanical hardness, among others [17].

Due to their high-density magnetic monitoring, these features make $CoFe_2O_4$ nanoparticles an appealing candidate for many magnetic necessities, like cameras, sensors, and electric motors [18]. Due to their medium saturation magnetization, outstanding chemical stability, low real part permittivity, and substantial magnetic loss, spinel ferrites (M Fe_2O_4, M = Fe, Co, Ni, Mn, Zn, etc.) are supposed as the proper candidates for microwave absorbing materials. Due to the single spinel ferrite microwave absorber's poor ability to attenuate, high density, quick aggregation, and tremendous covering thickness, getting into down-to-earth applications are genuinely challenging in any case. Then, the design of ferrite-based nanocomposites is of significant consideration for improving their microwave absorption efficiency [19]. In microwave absorption, carbon-based materials hold a wide variety of usages. Because of their remarkable physical and chemical characteristics, graphene, carbon nanotubes, graphite, and other carbon allotropic isomers are consequential in investigating microwave-absorbing materials [24–27]. Reduced graphene oxide (rGO) is a carbon-based substance employed in microwave absorbing materials as the ultralight one. To achieve lightweight absorbing materials, It's a practical way. The excellent carrier migration rate and dielectric constant of rGO distinguish it from other carbon-based materials. rGO is ultrathin, has a high optical transfer, and is stable at room temperature. Consequently, it has poor quality when used as a wave absorbing material, while it can lessen the skin effect impressively. Also, due to its specific surface area and fold form, rGO has a considerable resonance and interface polarization, advantageous for microwave absorbing and attenuating [28–32].

According to the supplementary effects on dielectric and magnetic characteristics, graphene/ferrite nanocomposites have gained a lot of interest in the latest years, especially given the broadband and lightweight expectations of absorbers. A $BaFe_{12}O_{19}@Fe_3O_4$ core-shell composite with a minor reflection loss (RL) of -33.6 dB at 11.6 GHz and 2.5 millimeters thick was synthesized by Lin et al. [19]. The lowest RL value of 29.7 decibel was reported by Bach et al. for a $La_{1.5}Sr_{0.5}NiO_4/NiFe_2O_4$ nanocomposites [20]. The min RL reached 58.4 decibels at 13.68 GHz with 2.1 millimeters thick for $Fe_3O_4/NiFe_2O_4$/Ni heterostructure porous rods, synthesized by Li et al. in a controllable way [21].

According to the supplementary effects on dielectric and magnetic characteristics, graphene/ferrite nanocomposites have gained a lot of interest in the latest years, especially given the broadband and lightweight expectations of absorbers. Meanwhile, numerous graphene/ferrite NCs have been generated using diverse techniques such as hierarchical $CoFe_2O_4$/rGO NCs with a porous structure which were synthesized employing an in-situ solvothermal technique and demonstrated a remarkable RL of -57.7 decibels with 2.8 millimeters thick [22]. Fe_3O_4/rGO hybrids holding the minimum RL of 22.7 decibels and a 3.13 GHz effective absorption bandwidth (90 percent absorption) were stated by Wu et al. [23]. By focusing on this perspective, nonstoichiometric $Co_{0.8}Fe_{2.2}O_4$ ferrite is chosen for this research to incorporate with rGO to produce $Co_{0.8}Fe_{2.2}O_4$/rGO NCs. The transmission line theory is used to assess the EM wave absorption characteristics of the recently prepared specimens. The microwave absorbing function of the composite materials is appropriately adjusted by modifying the rGO amount. In addition, the related EM wave absorbing mechanism of $Co_{0.8}Fe_{2.2}O_4$/rGO NCs is investigated.

2. Experimental

2.1. substances

LOBA in India formulated the natural graphite powder available in the market. Merck in Germany supplied H_2O_2 (30 weight percent), H_2SO_4 (99 weight percent), $KMnO_4$, Co $(NO_3)_2 \cdot 6H_2O$, $Cu(NO_3)_2 \cdot 6H_2O$ and $Fe(NO_3)_3 \cdot 9H_2O$, polyethylene glycol (PEG), as well as sodium acetate.

2.2. Graphene oxide's synthesis

The entire procedure for producing graphene oxide (GO) employing the modified Hummer's (MHM) technique brings as follows [33]: 4 grams of natural graphite were diffused thoroughly in 360 milliliters of H_2SO_4, 40 milliliters of H_3PO_4, and 18 grams of $KMnO_4$ were gently added. The combination was then dried at 60 degrees Celsius and shook for 12 hours. After chilling at room temperature, 200 milliliters of deionized water and 30% H_2O_2 solution were combined and shook till the solution acquired a brilliant yellow hue. The combination mentioned above was then centrifuged and thoroughly rinsed with deionized water, 30% HCl, and C_2H_5OH (ethanol) until the pH was approximately 6.

2.3. $Co_{0.5}Mn_{0.3}Cu_{0.2}Fe_2O_4$ NPs' preparation

In DI water, stoichiometric proportions of cobalt nitrate (Co $(NO_3)_2$), ferric nitrate (Fe $(NO_3)_3$), and also copper nitrate (Cu $(NO_3)_2$) are combined with ammonium hydroxide (NH_4OH) and citric acid ($C_6H_8O_7$). To achieve the transparent product, citric acid is utilized. Diverse doping percentages of copper nitrate employing the co-precipitation technique were controlled by the ammonium hydroxide synthesis. The precipitated components are filtered and then rinsed five times with distilled water. The ultimate precipitate material is dried for 8 hours at 120 degrees Celsius. The dried material is pulverized into a powder and set to sinter for 3 hours at 700 degrees Celsius. Ultimately, employing this method, the Cu doped Ba ferrite combination ($Co_{0.5}Mn_{0.3}Cu_{0.2}Fe_2O_4$) is acquired.

2.4. $Co_{0.5}Mn_{0.3}Cu_{0.2}Fe_2O_4$/rGO nanocomposites" manufacturing

The as-synthesized $Co_{0.5}Mn_{0.3}Cu_{0.2}Fe_2O_4$ NPs were diffused in GO colloid solution employing a common approach. The ultra-sonication bath was then used to stir the diffused $Co_{0.5}Mn_{0.3}Cu_{0.2}Fe_2O_4$ /rGO solution for 4 hours. After that, the specimen was dried at 80°C for 12 hours to generate $Co_{0.5}Mn_{0.3}Cu_{0.2}Fe_2O_4$/rGO composites. Ultimately, by heating them to 400°C for 3 hours, the Reduction process was applied to dried GO/ $Co_{0.5}Zr_{0.5}Fe_2O_4$ fabrics to obtain $Co_{0.5}Mn_{0.3}Cu_{0.2}Fe_2O_4$/rGO nanocomposites.

2.5. measurements and attributes

X-ray diffraction (X-ray Powder Diffraction, Bruker D 8 -Advance) with Cu K-α radiation (= 0.154 millimeters) was used to investigate as-synthesized Co0.8Fe2.2O4/rGO composites' crystallinity and

crystal structure. Nicolet NEXUS 670 Infrared Spectrometer analyzed FT-IR spectra between 400 to 4000 cm^{-1}. A scanning electron microscope (Flex SEM-1000) at 10 kilovolts was used to examine the microscopic morphology. An Agilent E8362B vector network analysis tool was used to test the EM variables (complex permittivity and complicated permeability) in the 2–18 GHz spectrum.

3. Discussion And Results

The XRD schemas of GO, $Co_{0.5}Mn_{0.3}Cu_{0.2}Fe_2O_4$, and $Co_{0.5}Mn_{0.3}Cu_{0.2}Fe_2O_4$/rGO composites are shown in Fig. 1. The diffraction apexes from X-ray Powder Diffraction schemas of $Co_{0.5}Mn_{0.3}Cu_{0.2}Fe_2O_4$ and $Co_{0.5}Mn_{0.3}Cu_{0.2}Fe_2O_4$/rGO at 2-theta = 18.5, 30.2, 35.6, 43.0, 53.5, 57.1, and 62.8 are consistent with the (111), (220), (311), (400), (422), (511), and (440) crystal surfaces of $Co_{0.5}Mn_{0.3}Cu_{0.2}Fe_2O_4$ (JCPDS numbers from 22 to 1086). This discovery demonstrates the cubic spinel form of $Co_{0.5}Mn_{0.3}Cu_{0.2}Fe_2O_4$ in the composite. The sharp apexes suggest that the manufactured $Co_0.8Fe_2.{}_2O_4$ NPs have excellent crystallinity [34, 35]. The intensity of the diffraction apexes for the $Co_{0.5}Mn_{0.3}Cu_{0.2}Fe_2O_4$ /rGO specimens appears to diminish compared to the $Co_{0.5}Mn_{0.3}Cu_{0.2}Fe_2O_4$ samples considerably, implying that the GO gain restrains the crystallinity of $CuFe_2O_4$ particles partially.

Figure 3 depicts the Fourier transform infrared (FTIR) ranges of unadulterated $Co_{0.5}Mn_{0.3}Cu_{0.2}Fe_2O_4$ and composite containing graphene specimens. The prominent apex at 1580 cm^{-1} may be ascribed to the stretching vibrancies of the not oxidized carbon skeleton.[36] Correspondingly, the O–H stretching and metamorphosis vibrancies are attributed to the bands at 3380 cm^{-1} and 1349 cm^{-1}. The bands at 1209 cm^{-1} and 1083 cm^{-1} are caused by epoxy category C–O and C–OH stretching vibrancies [37, 38]. The absorption apex at roughly 584 cm^{-1}, which is ascribed to the M–O band in cofe2o4, has been reported FTIR range of unadulterated $Co_{0.5}Mn_{0.3}Cu_{0.2}Fe_2\ O_4$, and the composite containing graphene specimens revealed effective GO reduction and pureness of the ternary metal oxide.

Scanning electron microscope captures of unadulterated $Co_{0.5}Mn_{0.3}Cu_{0.2}Fe_2\ O_4$ and graphene composite are shown in Fig. 3. The diameter of the agglomerated porous $Co_{0.5}Mn_{0.3}Cu_{0.2}Fe_2\ O_4$ nanostructures is 55 nanometers, as illustrated in Fig. 4a. Figure 4b. shows the SEM captures of Co0.5Mn0.3Cu0.2Fe2O4/rGO composites containing 40% graphene.

The magnetic hysteresis loops of unadulterated $Co_{0.5}Mn_{0.3}Cu_{0.2}Fe_2O_4$ and $Co_{0.5}Mn_{0.3}Cu_{0.2}Fe_2O_4$/rGO NCs at room temperature are shown in Fig. 4 in which all specimens exhibit ferromagnetic function. As indicated in Fig. 4, the saturation magnetizations (Ms) of the specimens $Co_{0.5}Mn_{0.3}Cu_{0.2}Fe_2O_4$ and $Co_{0.5}Mn_{0.3}Cu_{0.2}Fe_2O_4$/rGO 10 to 40 percent are reported as 80.1, 77.8, 73.6, 67.2 and 64.4 electromagnetic unit /gram, in the same order as mentioned. It is clear that Ms amount declines with GO amount growing due to the addition of nonmagnetic GO. Furthermore, as previously stated, the introduction of GO may effectively adjust the particle size, morphology, and microstructure of $Co_{0.5}Mn_{0.3}Cu_{0.2}Fe_2O_4$/rGO NCs, which has a significant impact on the magnetic characteristics of the as

synthesized composites. In the case of Magneto-crystalline anisotropy, form anisotropy, stress anisotropy, and exchange anisotropy influence the coercivity Hc of magnetic NPs again. Furthermore, deformation of the crystal lattice, local chemical disruption, and exchange interaction interruption all significantly affect the coercivity of NPs. The equivalent coercivity Hc values for specimens 1–5 are 1681, 613, 517, 764, 423, and 551 Oe. This research presents that as-synthesized nanocomposites adjust Hc due to the addition of GO, mainly due to the deformation of the crystal lattice, surface atoms' deviation, and changeable anisotropy.[40]

Moreover, based on the natural resonance equation, $2\pi fr = rHa$, and $Ha = 4|K1|/(3\mu 0Ms)$; in the same order as here, fr, r, Ha and |K1| equal the resonance frequency, the gyromagnetic ratio, the anisotropy energy, and anisotropy modulus. Consequently, magnetic NCs' natural resonance loss is mainly dictated by their magnetic characteristics. That seems to be the superior magnetic characteristics of as-synthesized NCs that help to enhance the EM wave absorption in the spectrum with low frequency.

Figure 5 depicts the frequency dependence of reflection loss at 2.0 mm thick, including all specimens. According to Fig. 5, the EM wave reflection loss is highly susceptible to the absorber's thickness. The RL apex shifts into a low frequency when the thickness increases. From an application perspective, a value of RL less than − 10 decibels is regarded as the threshold value due to the proper 90% EM wave absorption. The EM wave absorption performance of $Co_{0.5}Mn_{0.3}Cu_{0.2}Fe_2O_4$/rGO composites is clearly superior to that of the unadulterated $Co_{0.5}Mn_{0.3}Cu_{0.2}Fe_2O_4$ ferrite, as illustrated in Fig. 5. In the specimen $Co_{0.5}Mn_{0.3}Cu_{0.2}Fe_2O_4$, the minimum RL is -11.36 decibels at 12.5 GHz, whereas the effective absorbing bandwidth is 2.5 GHz. And the specimen $Co_{0.5}Mn_{0.3}Cu_{0.2}Fe_2O_4$/rGO 10% holds a min RL of 13.28 decibels at 14 GHz, equivalent to its effective absorbing bandwidth of 4.6 GHz. The specimen $Co_{0.5}Mn_{0.3}Cu_{0.2}Fe_2O_4$/rGO 20% has the best EM wave absorbing property, with a min RL of -20.2 decibels at 8.6 GHz and an absorbing bandwidth at 6.9 GHz. The $Co_{0.5}Mn_{0.3}Cu_{0.2}Fe_2O_4$/rGO 30% holds the maximum EM wave absorption property, with the min RL is -39.4 decibels at 11.5 GHz, and the absorption bandwidth is 6.8 GHz. Interestingly enough, The $Co_{0.5}Mn_{0.3}Cu_{0.2}Fe_2O_4$/rGO 40% demonstrates an extremely broad effective bandwidth, with the optimum absorbing bandwidth ranging from 8.7 to 18 GHz. At the same time, has 2.0 millimeters thick, and its min RL -25.2 is decibels.

Hereon, the as-synthesized $Co_{0.5}Mn_{0.3}Cu_{0.2}Fe_2O_4$/rGO composite indicates great EM wave absorbing capabilities, with premier reflection loss and an extremely wide effective absorption bandwidth, and there is no doubt about that.

4. Conclusion

To sum up, a two-step methodology was used to favorably manufacture $Co_{0.5}Mn_{0.3}Cu_{0.2}Fe_2O_4$/rGO nanocomposites. XRD, FT-IR, TEM, XPS, and VSM investigations were used to evaluate the constructional, morphological, surface analytical, and magnetic characteristics of nanocomposites. The Mn and Cu doped cobalt ferrite monotonously surrounded the surface of the rGO sheets, according to the

$Co_{0.5}Mn_{0.3}Cu_{0.2}Fe_2O_4$/rGO nanocomposites results. Moreover, measurements of microwave adsorption parameters indicate that the min RL of $Co_{0.5}Mn_{0.3}Cu_{0.2}Fe_2O_4$/rGO 40% nanocomposites may attain –25.2 dB at 12.7 GHz for a 2 mm thickness, and only 2 mm thickness in the effective absorption bandwidth (RL under 10 dB) spectrums from 8.7 to 18 GHz. As a result, $Co_{0.5}Mn_{0.3}Cu_{0.2}Fe_2O_4$ nanocomposites may be a wise option for microwave-absorbing materials.

Declarations

Funding: Not applicable.

Conflicts of interest/Competing interests: The authors declare that they have no known competing financial interests or personal relationships that could have appeared to influence the work reported in this paper.

Availability of data and material: Not applicable.

Code availability: Not applicable.

Authors' contributions (optional: please review the submission guidelines from the journal whether statements are mandatory**:** Not applicable.

Ethics approval: Not applicable.

Consent to participate: Not applicable.

Consent for publication: Not applicable.

Acknowledgements: Not applicable.

References

1. Y. Ding, Q.L. Liao, S. Liu, H.J. Guo, Y.H. Sun, G.J. Zhang, Y. Zhang, Reduced graphene oxide functionalized with cobalt ferrite nanocomposites for enhanced efficient and lightweight electromagnetic wave absorption, Sci. Rep. 6 (2016) 32381.
2. Y. Zhang, Y. Huang, T.F. Zhang, H.C. Chang, P.S. Xiao, H.H. Chen, Z.Y. Huang, Y.S. Chen, Broadband and tunable high-performance microwave absorption of an ultralight and highly compressible graphene foam, Adv. Mater. 27 (2015) 2049-2053.
3. W. Feng, Y.M. Wang, J.C. Chen, L.X. Guo, J.H. Ouyang, D.C. Jia, Y. Zhou, Microwave absorbing property optimization of starlike ZnO/reduced graphene oxide doped by ZnO nanocrystal composites, Phys. Chem. Chem. Phys. 19 (2017) 14596-14605.
4. F. Wang, X. Wang, J.F. Zhu, H.B. Yang, X.G. Kong, X. Liu, Lightweight NiFe2O4 with controllable 3D network structure and enhanced microwave absorbing properties, Sci. Rep. 6 (2016) 37892.

5. B. Shen, Y. Li, D. Yi, W.T. Zhai, X.C. Wei, W.G. Zheng, Microcellular graphene foam for improved broadband electromagnetic interference shielding, Carbon 102 (2016) 154–160.
6. P. Liu, Z. Yao, J. Zhou, Z. Yang, L.B. Kong, Small magnetic Co-doped NiZn ferrite/graphene nanocomposites and their dual-region microwave absorption performance, J. Mater. Chem. C 4 (2016) 9738-9749.
7. J. Feng, F.Z. Pu, Z.X. Li, X.H. Li, X.Y. Hu, J.T. Bai, Interfacial interactions and synergistic effect of CoNi nanocrystals and nitrogen-doped graphene in a composite microwave absorber, Carbon 104 (2016) 214-225.
8. T. Wu, Y. Liu, X. Zeng, T.T. Cui, Y.T. Zhao, Y.N. Li, G.X. Tong, Facile hydrothermal synthesis of Fe3O4/C core-shell nanorings for efficient low-frequency microwave absorption, ACS Appl. Mater. Interface 8 (2016) 7370-7380.
9. L.X. Wang, Y.K. Guan, X. Qiu, H.L. Zhu, S.B. Pan, M.X. Yu, Q.T. Zhang, Efficient ferrite/Co/porous carbon microwave absorbing material based on ferrite@metal-organic framework, Chem. Eng. J. 326 (2017) 945-955.
10. X. F. Liu, Y.X. Chen, X.R. Cui, M. Zeng, R.H. Yu, G.S. Wang, Flexible nanocomposites with enhanced microwave absorption properties based on Fe3O4/SiO2 nanorods and polyvinylidene fluoride, J. Mater. Chem. A 3 (2015) 12197-12204.
11. F. Shahzad, M. Alhabeb, C.B. Hatter, B. Anasori, S.M. Hong, C.M. Koo, Y. Gogotsi, Electromagnetic interference shielding with 2D transition metal carbides (MXenes), Science 353 (2016) 1137-1140.
12. J.Z. He, X.X. Wang, Y.L. Zhang, M.S. Cao, Small magnetic nanoparticles decorating reduced graphene oxides to tune the electromagnetic attenuation capacity, J. Mater. Chem. C 4 (2016) 7130-7140.
13. D. Moitra, S. Dhole, B.K. Ghosh, M. Chandel, R.K. Jani, M.K. Patra, S.R. Vadera, N.N. Ghosh, Synthesis and microwave absorption properties of BiFeO3 nanowire-RGO nanocomposite and first-principles calculations for insight of electromagnetic properties and electronic structures, J. Phys. Chem. C 121 (2017) 21290-21304.
14. Xiao-Juan Zhang, Guang-Sheng Wang, Wen-Qiang Cao, Wei Yun-Zhao, JunFei Liang, Lin Guo, Mao-Sheng Cao, Enhanced microwave absorption property of reduced graphene oxide (RGO)-MnFe2O4 nanocomposites and polyvinylidene fluoride, ACS Appl. Mater. Interfaces 6 (10) (2014) 7471–7478.
15. Y. Slimani, M.A. Almessiere, A. Demir Korkmaz, S. Guner, H. Güngünes¸, M. Sertkol, A. Manikandan, A. Yildiz, S. Akhtar, Sagar E. Shirsath, A. Baykal, Ni0.4Cu0.2Zn0.4TbxFe2-xO4 nanospinel ferrites: ultrasonic synthesis and physical properties, Ultrason. Sonochem. 59 (2019) 104757.
16. P. Liu, Z. Yao, J. Zhou, Preparation of reduced graphene oxide/ Ni0.4Zn0.4Co0.2Fe2O4 nanocomposites and their excellent microwave absorption properties, Ceram. Int. 41 (2015) 13409–13416.
17. M. Fu, Q. Jiao, Y. Zhao, Preparation of NiFe2O4nanorod–graphene composites via an ionic liquid assisted one-step hydrothermal approach and their microwave absorbing properties, J. Mater. Chem. 1 (2013) 5577–5586.

18. V. Sunny, P. Kurian, P. Mohanan, M.R. Anantharaman, A flexible microwave absorber based on nickel ferrite nanocomposite, J. Alloys Compd. 489 (2010) 297–303.
19. Y. Lin, Y. Liu, J. Dai, L. Wang, H. Yang, Synthesis and microwave absorption properties of plate-like BaFe12O19@Fe3O4 core-shell composite, J. Alloys Compd. 739 (2018) 202-210.
20. T.N. Bach, C.T.A. Xuan, N.T.H. Le, D.H. Manh, D.N.H. Nam, Microwave absorption properties of (100-x)La1.5Sr0.5NiO4/xNiFe2O4 nanocomposites, J. Alloys Compd. 695 (2017) 1658-1662.
21. Y. Li, T. Wu, K. Jin, Y. Qian, N. Qian, N. Qian, K. Jiang, W. Wu, G. Tong, Controllable synthesis and enhanced microwave absorbing properties of Fe3O4/NiFe2O4/Ni heterostructure porous rods, Appl. Surf. Sci. 387 (2016) 190-201.
22. Y. Liu, Z. Chen, Y. Zhang, R. Feng, X. Chen, C. Xiong, L. Dong, Broadband and lightweight microwave absorber constructed by in-situ growth of hierarchicalCoFe2O4/rGO porous nanocomposites, ACS Appl. Mater. Interf. 10 (2018) 13860.
23. J. Wu, Z. Ye, W. Liu, Z. Liu, J. Chen, The effect of GO loading on electromagnetic wave absorption properties of Fe3O4/reduced graphene oxide hybrids, Ceram. Int. 43 (2017) 13146-13153.
24. R.S. Yadav, I. Kuritka, J. Vilcakova, D. Skoda, P. Urbanek, M. Machovsky, M. Masar, L. Kalina, J. Havlica, Lightweight NiFe2O4-reduced graphene oxide-elastomer nanocomposite flexible sheet for electromagnetic interference shielding application, Compos. B Eng. 166 (2019) 95–111.
25. G.Y. Zhang, R.W. Shu, Y. Xie, H.T. Xia, Y. Gan, J.J. Shi, J. He, Cubic MnFe2O4 particles decorated reduced graphene oxide with excellent microwave absorption properties, Mater. Lett. 231 (2018) 209–212.
26. K.T. Kim, T.D. Dao, H.M. Jeong, A.V. Raghu, T.M. Aminabhavi, Graphene coated with alumina and its utilization as a thermal conductivity enhancer for alumina sphere/thermoplastic polyurethane composite, Mater. Chem. Phys. 153 (2015) 291–300.
27. T. Mathew, R.A. Sree, S. Aishwarya, K. Kounaina, A.G. Patil, P. Satapathy, S.P. Hudeda, S.S. More, K. Muthucheliyan, T.N. Kumar, A.V. Raghu, K.R. Reddy, F. Zameer, Graphene-based functional nanomaterials for biomedical and bioanalysis applications, FlatChem 23 (2020) 100184.
28. Q.C. Zhang, Z.J. Du, X.Z. Huang, Z.X. Zhao, T. Guo, G.J. Zeng, Y. Yu, Tunable microwave absorptivity in reduced graphene oxide functionalized with Fe3O4 nanorods, Appl. Surf. Sci. 473 (2019) 706–714.
29. K. Zhang, M.Q. Ye, A.J. Han, J.L. Yang, Preparation, characterization and microwave absorbing properties of MoS2 and MoS2 -reduced graphene oxide (RGO) composites, J. Solid State Chem. 277 (2019) 68–76.
30. D.P. Suhas, T.M. Aminabhavi, H.M. Jeong, A.V. Raghu, Hydrogen peroxide treated graphene as an effective nanosheet filler for separation application, RSC Adv. 5 (2015) 100984–100995.
31. H.B. Lee, A.V. Raghu, K.S. Yoon, H.M. Jeong, Preparation and characterization of poly(ethylene oxide)/graphene nanocomposites from an aqueous medium, J. Macromol. Sci. B 49 (2010) 802–809.

32. A.V.R.D.A. Nguyen, J.T. Choi, H.M. Jeong, Properties of thermoplastic polyurethane/functionalised graphene sheet nanocomposites prepared by the in situ polymerisation method, Polym. Polym. Compos. (2010) 351–358.
33. Y.F. Zhu, Q.Q. Ni, Y.Q. Fu, One-dimensional barium titanate coated multi-walled carbon nanotube heterostructures: synthesis and electromagnetic absorption properties, RSC Adv. 5 (2015) 3748.
34. K. Cai, W. Shen, B.Y. Ren, J. He, S.Z. Wu, W. wang, A phytic acid modified CoFe2O4 magnetic adsorbent with controllable morphology, excellent selective adsorption for dyes and ultra-strong adsorption ability for metal ions, Chem. Eng. J. 330 (2017) 936-946.
35. R. Chen, W. Wang, X. Zhao, Y. Zhang, S. Wu, F. Li, Rapid hydrothermal synthesis of magnetic CoxNi1-xFe2O4 nanoparticles and their application on removal of Congo red, Chem. Eng. J. 242 (2014) 226-233.
36. H. K. Jeong, Y. P. Lee, R. J. W. E. Lahaye, M. H. Park, K. H. An, I. J. Kim, C. W. Yang, C. Y. Park, R. S. Ruoff, Y. H. Lee, Evidence of graphitic AB stacking order of graphite oxides, J. Am. Chem. Soc., 2008, 130, 1362–1366.
37. M. Acik, G. Lee, C. Mattevi, M. Chhowalla, K. Cho, Y. J. Chabal, Unusual infrared-absorption mechanism in thermally reduced graphene oxide, Nat. Mater., 2010, 9, 840–845.
38. Y. Fu and X. Wang, Magnetically Separable ZnFe2O4–Graphene Catalyst and its High Photocatalytic Performance under Visible Light Irradiation, Ind. Eng. Chem. Res., 2011, 50, 7210–7218.

Figures

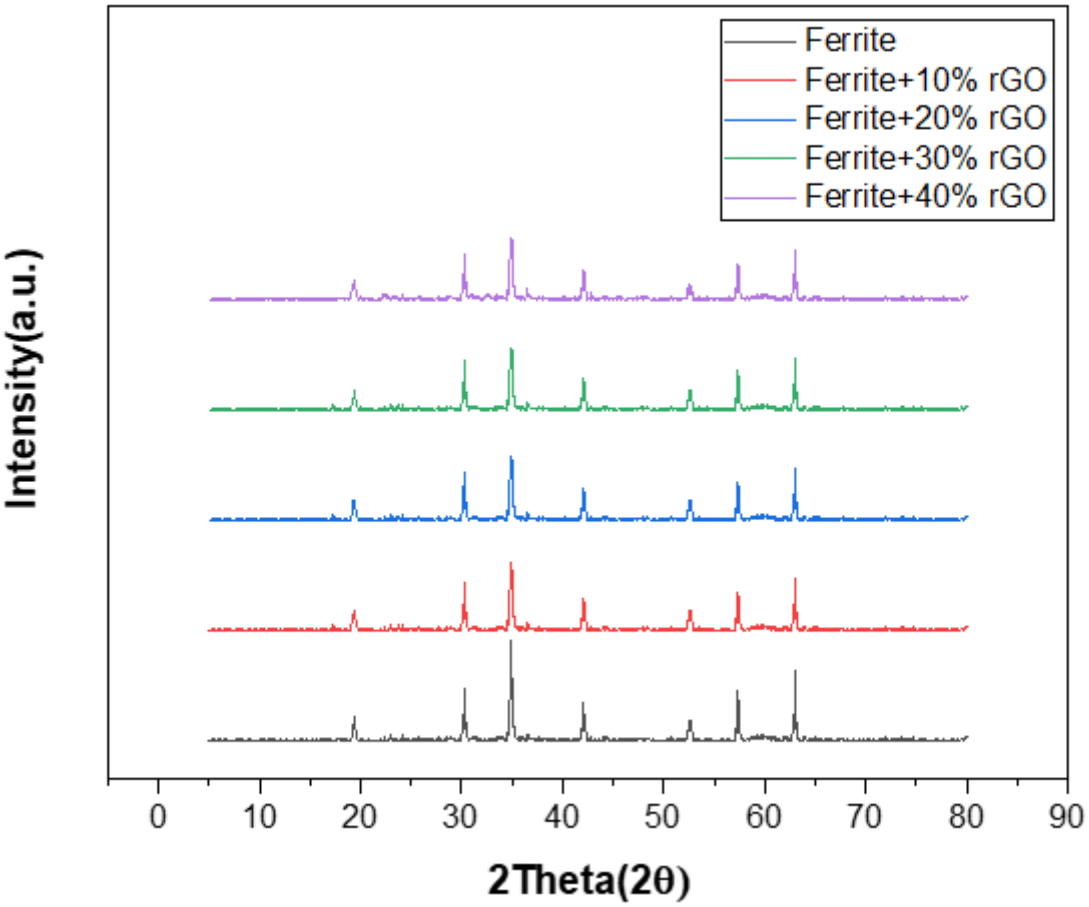

Figure 1

X-Ray Diffraction (XRD) schemas of $Co_{0.5}Mn_{0.3}Cu_{0.2}Fe_2O_4$ and $Co_{0.5}Mn_{0.3}Cu_{0.2}Fe_2O_4$/rGO.

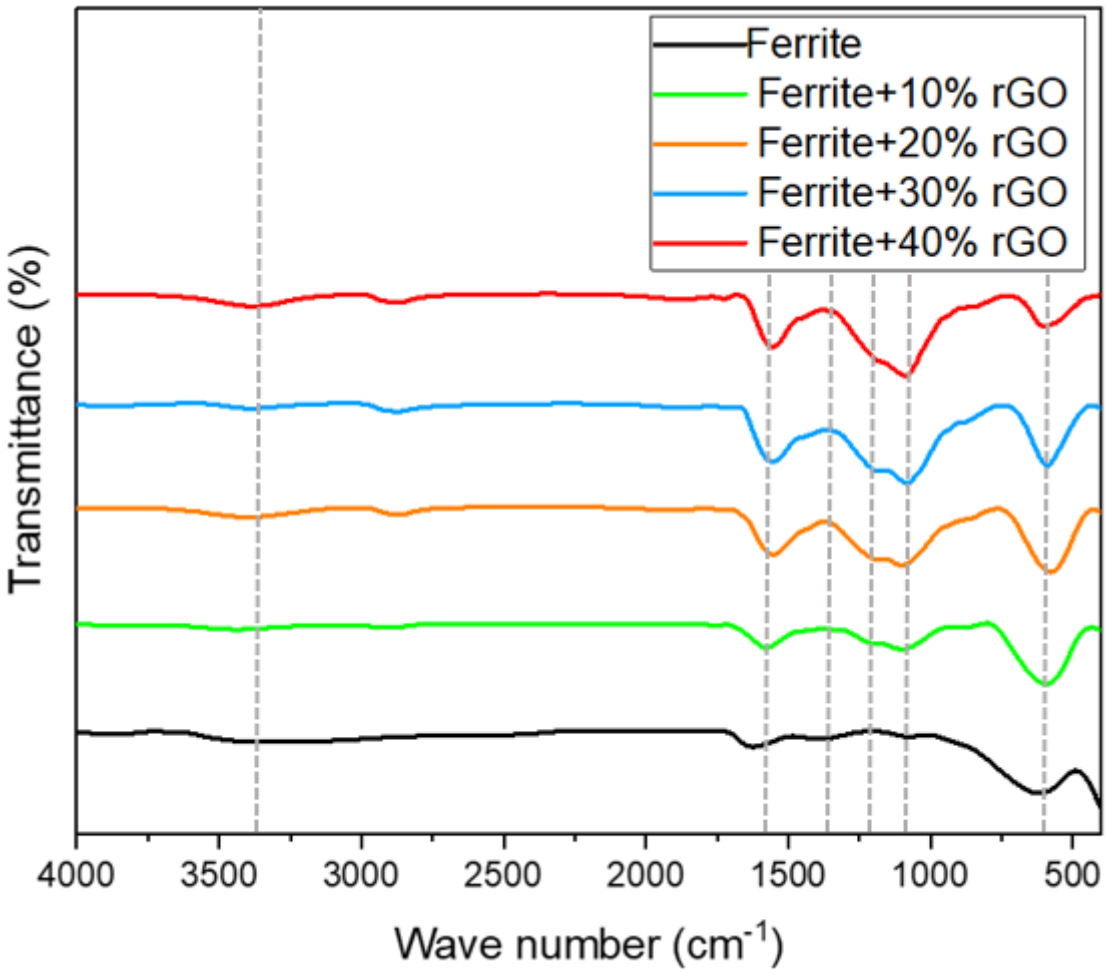

Figure 2

Fourier-transform infrared spectroscopy (FTIR) schemas of $Co_{0.5}Mn_{0.3}Cu_{0.2}Fe_2O_4$ and $Co_{0.5}Mn_{0.3}Cu_{0.2}Fe_2O_4$/rGO.

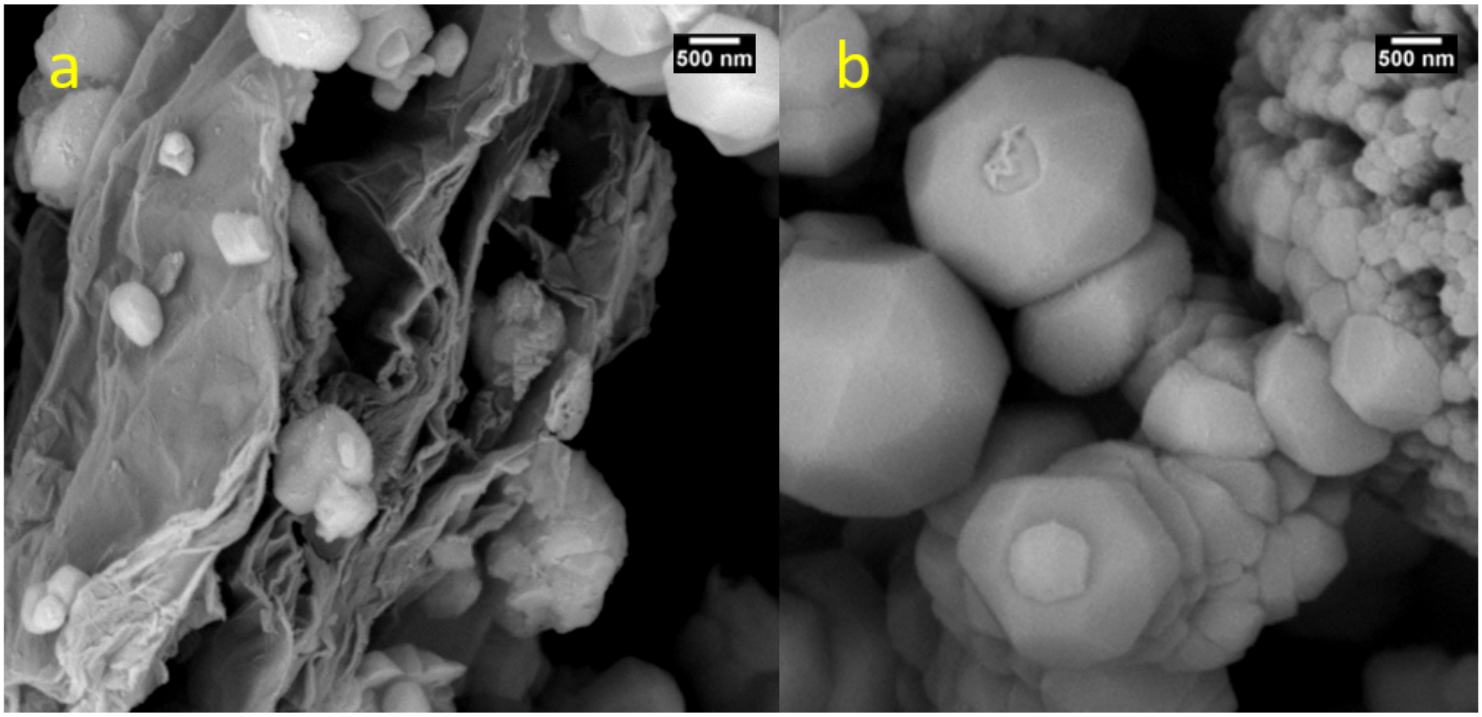

Figure 3

Scanning electron microscopy images of $Co_{0.5}Mn_{0.3}Cu_{0.2}Fe_2O_4$ + 40% rGO (a) and unadulterated $Co_{0.5}Mn_{0.3}Cu_{0.2}Fe_2O_4$ (b).

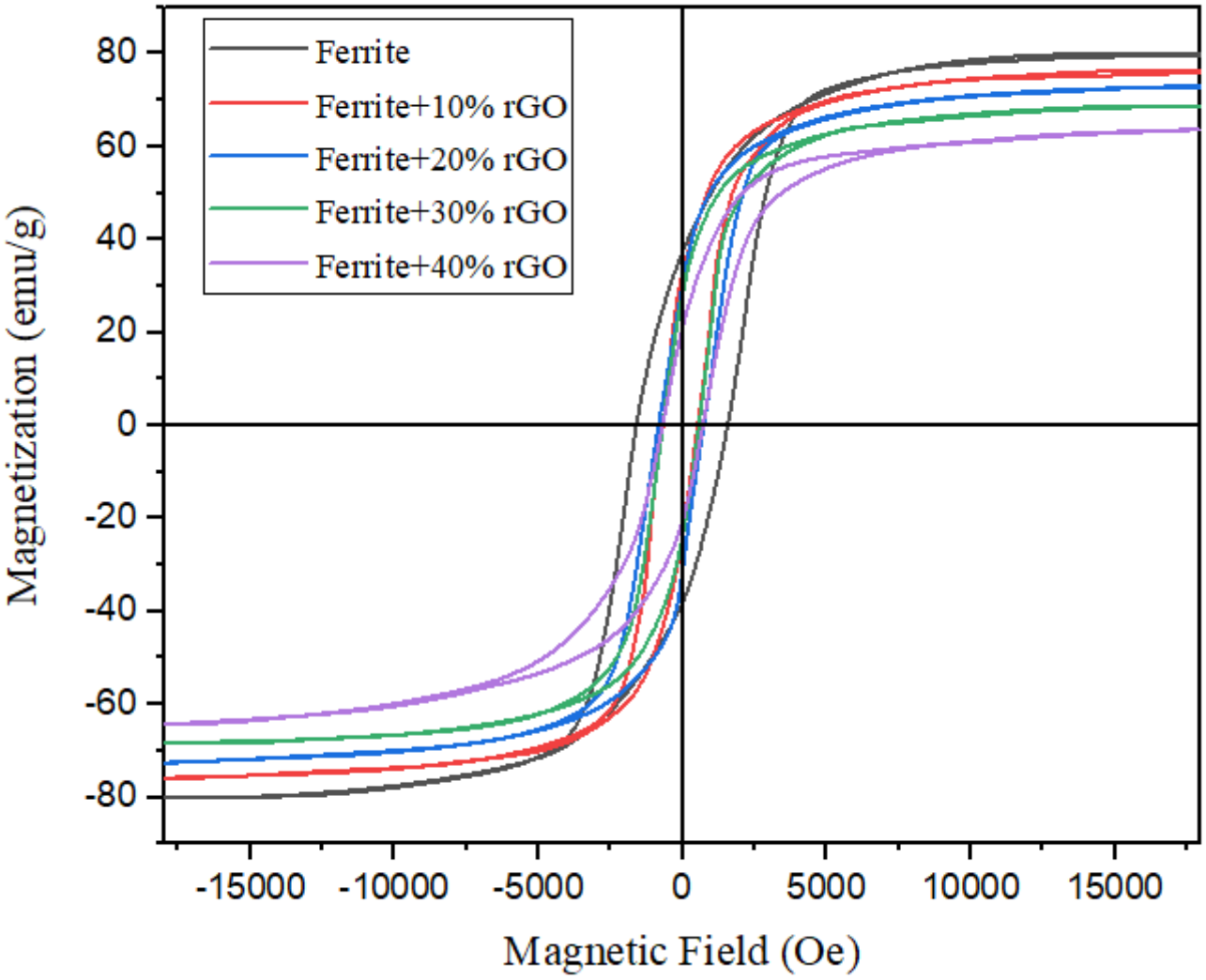

Figure 4

Specimen's hysteresis loops at room temperature.

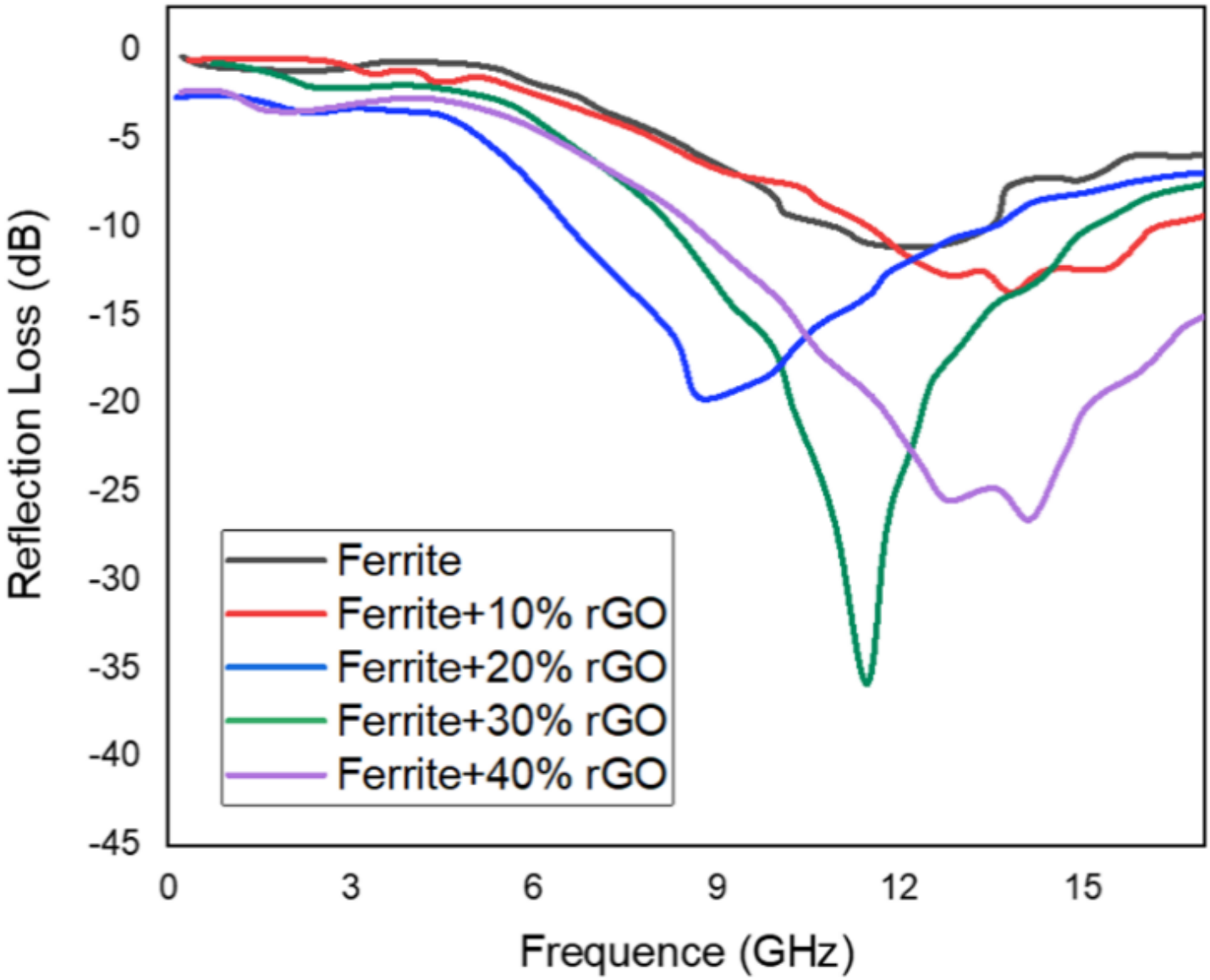

Figure 5

Specimen's reflection loss